Final version available at: https://doi.org/10.1109/TIE.2018.2822618

LED Series Current Regulator Based on a Modified Class-E Resonant Inverter

Javier Ribas, *Senior Member, IEEE*, Pablo J. Quintana-Barcia, *Member, IEEE*, Jesus Cardesin, *Member, IEEE*, Antonio J. Calleja, *Senior Member, IEEE*, and Emilio Lopez Corominas, *Member, IEEE*

***Abstract*—This paper presents a new topology based on a modified class-E resonant inverter used as an LED series current regulator. The proposed topology behaves as a controllable nondissipative impedance that adjusts the current flowing through the lamp. In this circuit, the LED is placed at the dc side of the class-E inverter, in series with the input filter inductance. The power handled by the ac side is sent back to the input by means of two diodes. Despite the addition of these two diodes, the converter maintains all the advantages of the class-E inverter: low component count, simple control, and extremely low switching losses. The LED current can be controlled with a small variation of the operating frequency. This way, the low-frequency current ripple of the lamp can be strongly reduced even when there is a considerably high input voltage excursion, such as the one expected in electrolyticless high-power-factor LED ballast. This paper proposes a simplified methodology based on the fundamental approach aiming to design and build a laboratory prototype. The prototype is designed in order to minimize the effect of LED voltage in the output current. This way, the input voltage ripple can be canceled using a simple feedforward control.**

***Index Terms*—Class-E inverter, LED driver, resonant power conversion.**

I. Introduction

REPLACEMENT of high-intensity discharge (HID) lamps by LED-based fixtures in public lighting systems is taking place at a slower pace compared to most other lighting applications. Only in the last few years, the efficiency increase, combined with the cost reduction, better performance, and improved durability of the electronic drives, have turned the LED into an interesting alternative. For example, in Europe, the most commonly used HID lamps for street lighting are high-pressure sodium and metal halide lamps in the 150–400 W range. These lamps have a life expectancy between 10 000 and 25 000 h and efficiencies between 60 and 120 lm/W. Currently, LED lamps can last more than 50 000 h with a light output above 80% of the nominal [1]. But even if that time is exceeded, the lamp will not fail to start, as it would happen with HID lamps. That is an important feature for street lighting, where a lamp failure could compromise people's safety. On the other hand, nowadays they can be found in the market, LEDs with efficiencies above 180 lm/W and high-power LED chips that can be used to design compact light sources as required for street lighting. Another interesting feature of LED lamps is that they are easily dimmed. In comparison, reducing the current in HID lamps has a very detrimental effect on the electrode operating temperature producing much shorter lifetimes.

LED-based luminaires have to be designed in a completely different way compared to HID-based ones. One of the main reasons is the high directivity of LEDs that allows a more efficient use of the light, reducing the reflector losses present in standard HID luminaires. Another critical characteristic of LED lamps is thermal management. Light output and life expectancies of the lamp and drive are directly related to the operating temperature. One of the key elements to determine the life of the electronic drive is the bulk capacitor required for power factor correction (PFC). As can be found in [2] and [3], there are two solutions to extend the life of this capacitor. The first one is using a high-temperature electrolytic capacitor operating far below its maximum rated temperature [4]. This way, the evaporation of the liquid electrolyte is strongly reduced allowing to extend capacitor life above 50 000 h. This is the most commonly used strategy in currently available LED ballasts in the market. The other solution is replacing the electrolytic capacitor with a plastic one [5]–[8]. This second solution requires a special design of the power topology in order to reduce the size of this capacitor to a suitable value. These designs normally provide a higher low-frequency ripple at the output of the PFC stage, thus making necessary the use of a second stage to reduce the LED current ripple to an acceptable level [2], [9]. The present work proposes a new topology specially designed to be used as a second stage in this kind of solution.

To achieve the lighting levels required for public lighting systems, arrangements with multiple LED strings are normally used. As the operating voltage of each individual LED may vary, current flowing through these strings must be equalized

Manuscript received September 28, 2017; revised December 19, 2017 and February 13, 2018; accepted March 11, 2018. This work was supported in part by the Ministry of Economy and Competitiveness of the Government of Spain, in part by the Government of the Principado de Asturias, and in part by the European Union through the European Regional Development Fund under Research Grant ENE2013-41491-R and Grant GRUPIN14-076. *(Corresponding author: Javier Ribas.)*

The authors are with the Efficient Energy Conversion, Industrial Electronics and Lighting Group, University of Oviedo, 33204 Gijon, Spain (e-mail: ribas@uniovi.es; quintanapablo@uniovi.es; cardesin@uniovi.es; calleja@uniovi.es; elopezc@uniovi.es).

Color versions of one or more of the figures in this paper are available online at http://ieeexplore.ieee.org.

Digital Object Identifier 10.1109/TIE.2018.2822618

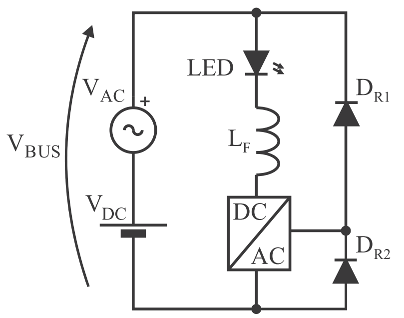

Fig. 1. Basic operation of the series current regulator.

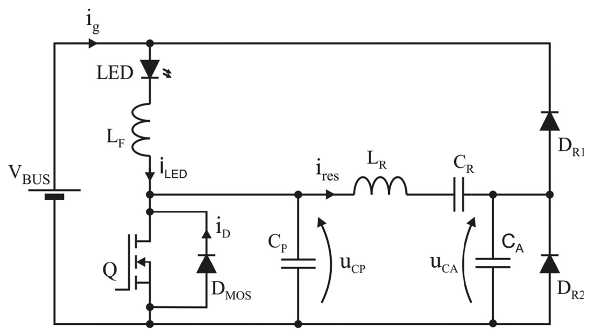

Fig. 2. Simplified schematics of the proposed circuit.

[10], [11]. In the recent literature, several solutions to achieve the double goal of reducing the low-frequency ripple and equalizing the LED current were presented [12]–[14].

In the present work, a new topology based on an LED series current regulator is proposed. The circuit is based on a resonant inverter whose input is placed in series with the LED lamp and the energy handled by the ac output is rectified and sent back to the input, as shown in Fig. 1. This way, the converter behaves as an adjustable dc impedance that can be used to control the LED current. In this configuration, the amount of power processed by the inverter is directly related to the difference between V_{BUS} input and LED voltages. If this difference is small, the power recycled by this stage will be small. Therefore, this approach is especially suited for applications where the input voltage is not far from the LED voltage [6], [15].

In this work, the dc–ac stage is a class-E resonant inverter. Replacing the dc to ac block shown in Fig. 1 with a class-E inverter, the circuit in Fig. 2 is obtained.

The circuits proposed in the bibliography as second stages for LED ballasts can be classified as nonresonant [12], [13], [28] and resonant [19], [26], [27]. Nonresonant solutions, such as the buck converter, are the most simple and versatile, but hard switching limits the maximum frequency that is achievable without compromising converter efficiency; thus, the size of the converter can hardly be optimized, even considering the low component count that these converters have. Resonant converters can be used to reduce switching losses and increase the operating frequency. Some of the solutions found in the bibliography are based on the *LLC* resonant inverter followed by a rectifier [26], [27]. The switching losses in these circuits can be extremely small. Another interesting feature is that the voltage stress in the switches is limited to the input voltage. The main disadvantage is that two transistors are required, increasing the complexity and cost of both the power converter and the control circuit. Another circuit configuration that can be found in the bibliography consists of a class-E inverter followed by a rectifier [19]. This solution has some similarities with the proposed circuit that is described next.

The class-E resonant converter is a single switch topology especially suited to operate at very high frequencies due to its inherent low switching losses [16], [17]. The capacitor placed in parallel with the switch ensures a small dv/dt reducing the turn-OFF losses. Besides, if the ZVS condition is met, the turn-ON losses will also be extremely small. This characteristic allows the use of switching frequencies of several megahertz in certain applications of this topology [16], [23]. One of the main disadvantages of the class-E converter is the high ratio between the peak and average voltages across the switch. Peak MOSFET voltage values 3–7 times higher than the input are easily obtained. Another disadvantage of this topology is that if the ZVS condition is lost and the switch turns ON before the capacitor is fully discharged, high current spikes will appear and efficiency will be severely reduced. Class-E converters can be controlled by modifying the switching frequency [18].

Control and design must be made taking into account that the ZVS condition has to be maintained for all possible operating conditions [17], [20].

The most significant difference between proposed circuit and the class-E resonant converter in [19] is that the equivalent input voltage of the class-E inverter block in the proposed solution is equal to the bus voltage minus the LED voltage, significantly reducing the voltage stress in the switch. This circuit can be used instead of low-voltage-drop linear regulators to control LED current through different branches (as in [14]). If the input and LED voltages are similar, current control or equalization among branches can be made with an extremely high efficiency.

However, the proposed circuit can also be used with higher input-to-output voltage differences. To illustrate this, the circuit described in the design example section provided a constant 40 W output power using a 160 V input bus with a 100 Hz peak-to-peak ripple of 37.5%. If the PFC input stage works as an ideal resistance simulator, this ripple could be obtained using a $14\,\mu\mathrm{F} - 200\,\mathrm{V}$ bulk capacitor in the dc bus [28]. This can be easily achieved using a flyback or a buck–boost input stage.

The remainder of the paper is organized as follows. First, a detailed description of the converter operation is made. Second, the basic equations and design charts are obtained using the fundamental approach to model circuit behavior. After that and based on the previous analysis, a straightforward design methodology is proposed. To further improve the design criteria, a sensitivity analysis is carried out in the next paragraph. Finally, a design example with its corresponding experimental results and conclusions are presented.

II. Circuit Operation

Fig. 3 shows the basic waveforms of the circuit previously depicted in Fig. 2. To simplify the analysis, the resonant current

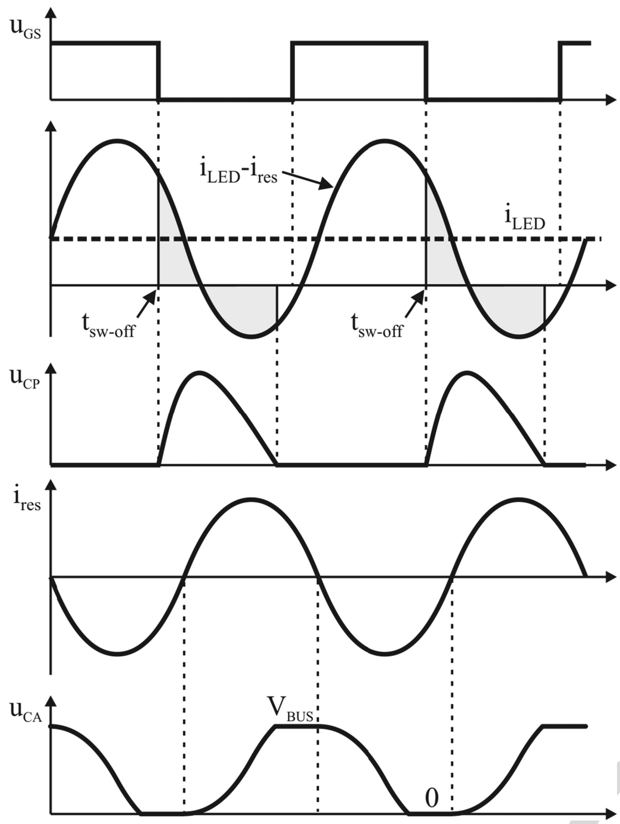

Fig. 3. Basic waveforms of the proposed modified class-E series regulator.

i_{res} is assumed to be perfectly sinusoidal and the LED current ripple is neglected. The study of the circuit is divided into two parts. The MOSFET voltage waveform (u_{CP}) as a function of $i_{\text{res}}, i_{\text{LED}}$ and the relative phase-shift of the switch-OFF instant ($t_{\text{sw-off}}$) are obtained in the first part. On the other hand, the truncated waveform of the capacitor C_A (u_{CA}) is studied in the second part.

When the transistor switches OFF, the current $i_{\text{LED}} - i_{\text{res}}$ starts flowing through capacitor C_P. The maximum voltage in this capacitor is reached at the zero crossing of $i_{\text{LED}} - i_{\text{res}}$ current. After that, u_{CP} voltage decreases until the intrinsic MOSFET diode is forward biased. The transistor must be switched ON at this interval to ensure ZVS operation. Duty cycle changes within this margin have a negligible effect on circuit waveforms. As shown in Fig. 3, u_{CP} signal has strong harmonic content and a high peak-to-average ratio.

Besides, voltage u_{CA} is limited between V_{BUS} and zero by diodes D_{R1} and D_{R2}. When the resonant current i_{res} changes from negative to positive, diode D_{R2} turns OFF and voltage u_{CA} starts to increase. When it reaches V_{BUS}, diode D_{R1} turns ON and part of the energy handled by the resonant tank is delivered to the input.

III. Simplified Analysis Using the Fundamental Approach

The equations that define the circuit behavior are obtained in four steps.

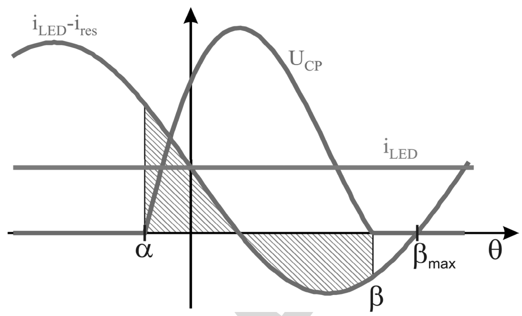

Fig. 4. Operation of the class-E inverter using the fundamental approach.

1) Calculation of the equations given by the charge and discharge of capacitors C_P and C_A.
2) Class-E inverter power balance.
3) Zero average voltage across the filter inductance L_F.
4) Analysis of the fundamental component of voltage and current in the resonant tank $L_R - C_R$.

To analyze the voltage waveform across capacitor C_P, the phase reference that is used is the zero crossing of the resonant current i_{res}. Angle α is defined as the switch turn-OFF instant and angle β is the point where C_P fully discharges (see Fig. 4). According to the circuit operation described in the previous paragraph, positive and negative shaded areas in Fig. 4 must be equal. Assuming a sinusoidal resonant current with a peak value of $I_{\text{res(peak)}}$ and an angular frequency ω, the evolution of u_{CP} as a function of time inside a reference period defined as $-T/2$ to $T/2$ can be calculated using the following equation, where T is the switching period:

$$U_{\text{CP}}\ (t) = \begin{cases} \frac{1}{C_P} \int_{\alpha/\omega}^{t} \left(i_{\text{LED}} - I_{\text{res(peak)}} \cdot \sin\left(\omega \cdot t_a\right)\right) \cdot dt_a, & \text{if } \frac{\alpha}{\omega} < t < \frac{\beta}{\omega} \\ 0, & \text{otherwise} \end{cases}. \tag{1}$$

Defining q as the ratio between the LED current i_{LED} and the peak value of the resonant current $i_{\text{res(peak)}}$

$$q\ = \frac{i_{\text{LED}}}{I_{\text{res(peak)}}}. \tag{2}$$

In addition, the normalized expression of C_P capacitor voltage can be defined as follows:

$$M_{\text{CP}}\ (\theta) = \begin{cases} \int_{\alpha}^{\theta} \left(q - \sin\left(\theta_a\right)\right) \cdot d\theta_a, & \text{if} \quad \alpha < \theta < \beta \\ 0, & \text{otherwise} \end{cases}. \tag{3}$$

The relation between (3) and (1) is given by

$$U_{\text{CP}}\left(\theta\right) = \frac{I_{\text{res(peak)}}}{C_P \cdot \omega}\, M_{\text{CP}}\left(\theta\right). \tag{4}$$

The expression of the angle β, which sets the point where C_P fully discharges, is

$$\int_{\alpha}^{\beta} \left(q - \sin\left(\theta_a\right)\right) \cdot d\theta_a \,=\, 0. \tag{5}$$

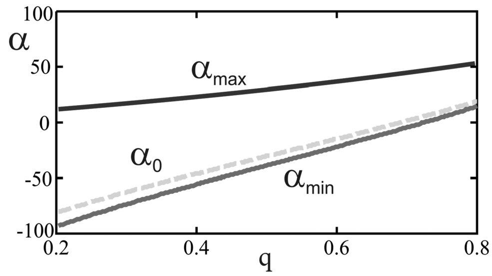

Fig. 5. Theoretical α limits.

Its maximum value is limited by the zero crossing with the positive slope of the $i_{\mathrm{LED}} - \mathrm{i_{res}}$ current. Higher β values will make it impossible to completely discharge the C_P capacitor before the transistor switches ON. This maximum angle can be calculated as follows:

$$\beta_{\max}\ (q) = \ \pi - \sin^{-1}(q). \tag{6}$$

Besides, the minimum α value is found when β reaches its maximum value. Combining (3) and (6), this switch turn-OFF angle is obtained

$$\cos(\alpha_{\min}(q)) + q \cdot \sin^{-1}(q) - \pi \cdot q + \alpha_{\min}(q) \cdot q + \sqrt{1-q^2} = 0. \tag{7}$$

The maximum α and the minimum β values will be reached when α equals β, that is

$$\alpha_{\max}\ (q) = \sin^{-1}(q). \tag{8}$$

To operate with ZVS, the transistor must be switched ON between β and $\beta_{\max}$. The difference between these two values determines the maximum and minimum duration of the switch ON time. If these two values are too close, the control margin will be excessively narrow. Therefore, a new design parameter δ is introduced in (9) as the percentage of the desired α value (α_0) related to its minimum and maximum values. If the selected δ is equal to zero, α will be minimum, and if it is 100, it will be maximum. Fig. 5 represents the α limits given by (7) and (8) and the desired value of (9) for a δ reference value of 10%:

$$\alpha_0\ (q) = \alpha_{\min}\ (q) \cdot \left(1 - \frac{\delta}{100}\right) + \alpha_{\max}(q) \cdot \frac{\delta}{100}. \tag{9}$$

As aforementioned, one of the limiting factors when designing a class-E inverter is the peak-to-average voltage ratio across the switch. This ratio can be numerically calculated using (3) and (9) and depicted as a function of q and δ parameters, as shown in Fig. 6. As can be seen, to reduce this ratio, low values of q and δ should be chosen. But low δ values also mean smaller control margin to achieve ZVS. This margin is defined as $\beta_{\max} - \beta$, and it can be calculated combining (5) and (6), as shown in Fig. 7. In most applications, a $\beta_{\max} - \beta$ margin around 30° would be enough to ensure ZVS; thus, a δ value of 10% is chosen as a reference design value.

The voltage across capacitor C_A can be calculated taking into account that this part of the circuit behaves as a capacitor driven by a sinusoidal current whose maximum and minimum voltages are set by two clamping diodes D_{R1} and D_{R2}. When the resonant current becomes positive, diode D_{R2} is reverse biased and capacitor C_A charges until the condition (10) is met. The angle where V_{BUS} voltage is reached is denoted as ξ (see Fig. 8):

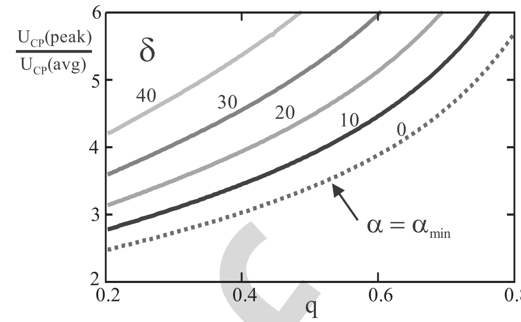

Fig. 6. Peak to average voltage ratio across the MOSFET.

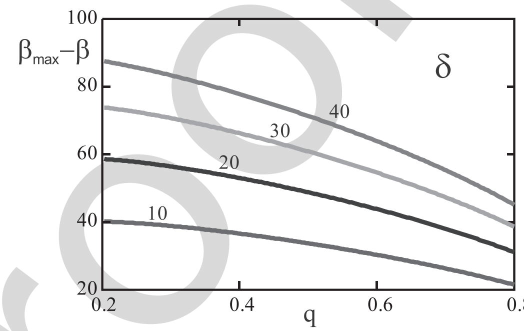

Fig. 7. MOSFET inverse current conduction angle for ZVS.

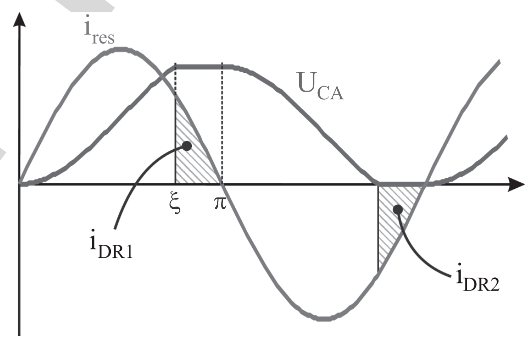

Fig. 8. Operation of the ac power recycling circuit.

$$V_{\mathrm{BUS}} = \frac{1}{C_A \cdot \omega} \int_0^{\xi} I_{\mathrm{res(peak)}} \cdot \sin(\theta_a) \cdot d\theta_a. \tag{10}$$

Between ξ and π, u_{CA} voltage is equal to V_{BUS}. The evolution when i_{res} is negative is symmetrical; thus, the following equation can be used to describe the evolution of the normalized C_A voltage:

$$M_{\mathrm{CA}}\ (\theta) = \begin{cases} 1 - \cos(\theta), & \text{if} \quad 0 < \theta < \xi \\ 1 - \cos(\xi), & \text{if} \quad \xi < \theta < \pi \\ -\cos(\xi) - \cos(\theta), & \text{if} \quad \pi < \theta < \pi + \xi \\ 0, & \text{if} \quad \pi + \xi < \theta < 2\pi \end{cases}. \tag{11}$$

The relation between the normalized value and the actual one is given by

$$U_{\mathrm{CA}}(\theta) = \frac{I_{\mathrm{res(peak)}}}{C_A \cdot \omega} M_{\mathrm{CA}}(\theta). \tag{12}$$

The second step of the analysis is made using the inverter power balance. The average voltage across the switch ($V_{\mathrm{BUS}} - \mathrm{V}_{\mathrm{LED}}$) multiplied by the LED current (i_{LED}) can be used to calculate the inverter input power. From the integration of the current i_{DR1} during a switching period and its multiplication by V_{BUS}, the output power can be calculated. Assuming there is no power loss, the input and output powers must be equal. Then, the following equation is obtained:

$$\frac{1}{2\pi}\int_{\xi}^{\pi} I_{\mathrm{res(peak)}} \cdot V_{\mathrm{BUS}} \cdot \sin(\theta_a) \cdot d\theta_a = (V_{\mathrm{BUS}} - V_{\mathrm{LED}}) \cdot I_{\mathrm{LED}}. \tag{13}$$

Defining parameter κ as the ratio

$$\kappa = \frac{V_{\mathrm{BUS}}}{V_{\mathrm{LED}}}. \tag{14}$$

Equation (13) can therefore be simplified if combined with (14) and expressed as

$$\cos(\xi) = 2\pi \cdot \left(1 - \frac{1}{\kappa}\right) \cdot q - 1. \tag{15}$$

Using the zero-average voltage condition across the filter inductance L_F, another design equation can be obtained. This way, $V_{\mathrm{BUS}} - \mathrm{V}_{\mathrm{LED}}$ must be equal to the average switch voltage calculated integrating (3):

$$V_{\mathrm{BUS}} - V_{\mathrm{LED}} = \frac{I_{\mathrm{res(peak)}}}{C_P \cdot \omega} \cdot \frac{1}{2\pi}\int_{\alpha}^{\beta} q \cdot (\theta_a - \alpha) + (\cos(\theta_a) - \cos(\alpha)) \cdot d\theta_a. \tag{16}$$

If the LED equivalent resistance is denoted as R

$$R = \frac{V_{\mathrm{LED}}}{I_{\mathrm{LED}}}. \tag{17}$$

Equation (16) can be rewritten as

$$R \cdot \omega \cdot C_P = \frac{1}{q \cdot (\kappa - 1)} \cdot \frac{1}{2\pi}\int_{\alpha}^{\beta} q \cdot (\theta_a - \alpha) + (\cos(\theta_a) - \cos(\alpha)) \cdot d\theta_a. \tag{18}$$

At this point, another important relation can be obtained analyzing the charging interval of capacitor C_A. Based on (10) and using the parameter definitions (2), (14), and (17) together with (15), the following equation is obtained:

$$R \cdot \omega \cdot C_A = \frac{1}{q \cdot \kappa} \cdot \left(2 - 2\pi \cdot \left(1 - \frac{1}{\kappa}\right) \cdot q\right). \tag{19}$$

The last step of the analysis uses the continuous Fourier transform to calculate i_{res} as a function of the fundamental component of the voltage applied to the resonant tank L_R–C_R. The voltage waveforms of u_{CP} and u_{CA} are given by (3) and (11); thus, to calculate the voltage across the resonant tank, the difference between the fundamental components of both signals is used:

$$\langle U_{\mathrm{CP}}\rangle_1 - \langle U_{\mathrm{CA}}\rangle_1 = \frac{I_{\mathrm{res(peak)}}}{C_P \cdot \omega}\langle M_{\mathrm{CP}}\rangle_1 - \frac{I_{\mathrm{res(peak)}}}{C_A \cdot \omega}\langle M_{\mathrm{CA}}\rangle_1. \tag{20}$$

This voltage divided by the impedance of the resonant tank formed by L_R and C_R is used to calculate the value of i_{res}.

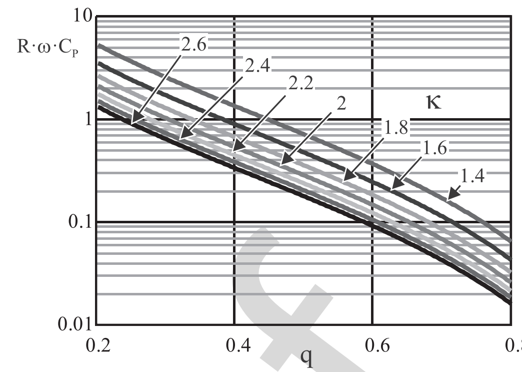

Fig. 9. Calculation of the C_P capacitor.

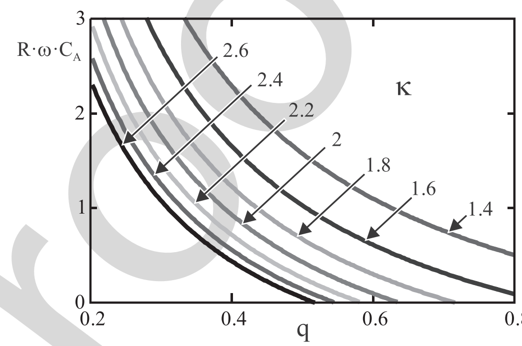

Fig. 10. Calculation of the C_A capacitor.

IV. Obtaining the Steady-State Design Charts

The proposed design procedure consists of obtaining the values of C_P, C_A, C_R, and L_R as functions of the design parameters defined in the previous paragraph (i.e., α, q, and κ), the constraints given by LED equivalent impedance R and the operating frequency ω. To obtain C_P, (18) is used. This expression gives the value of $R \cdot \omega \cdot C_P$ as a function of α, q, and κ. Therefore, a function $F1$ is defined as follows:

$$R \cdot \omega \cdot C_P = F1(\alpha, q, \kappa). \tag{21}$$

As was previously stated, the design value selected for parameter δ is 10%, whereas α is obtained as a function of q using (9). Fig. 9 shows the numerical solution of (21) as a function of q for different values of κ.

In a similar way, (19) gives $R \cdot \omega \cdot C_A$ as a function of q and κ; thus, a function $F2$ is defined as

$$R \cdot \omega \cdot C_A = F2(q, \kappa). \tag{22}$$

The numerical solution of this equation is shown in Fig. 10. This chart is used to calculate C_A.

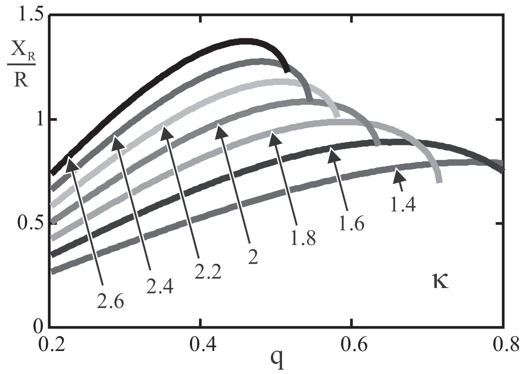

Fig. 11. Calculation of $L_R - C_R$ impedance.

If the impedance of the resonant tank is denoted as X_R, (20)–(22) can be combined into

$$\frac{X_R}{R} = \frac{\langle M_{\mathrm{CP}} \rangle_1}{F1\,(\alpha, q, \kappa)} - \frac{\langle M_{\mathrm{CA}} \rangle_1}{F2\,(q, \kappa)}. \tag{23}$$

This equation is rewritten defining an additional function *Fi*

$$\frac{X_R}{R} = Fi\,(\alpha, q, \kappa)\,. \tag{24}$$

The numerical solution of this expression is shown in Fig. 11. To calculate the values of L_R and C_R, an additional parameter ν is defined as the ratio between the impedance of both the components:

$$\nu = \frac{X_{LR}}{X_{CR}} = \omega^2 \cdot L_R \cdot C_R. \tag{25}$$

This parameter ν allows defining two new functions *F*3 and *F*4 to calculate L_R and C_R:

$$R \cdot \omega \cdot C_R = \frac{(\nu - 1)}{Fi\,(\alpha, q, \kappa)} = F3\,(\alpha, q, \kappa, \nu) \tag{26}$$

$$\frac{\omega \cdot L_R}{R} = \frac{Fi\,(\alpha, q, \kappa) \cdot \nu}{(\nu - 1)} = F4\,(\alpha, q, \kappa, \nu)\,. \tag{27}$$

V. Linearization

The equations and charts obtained in the previous section are intended to choose suitable design values for C_P, C_A, C_R, and L_R at the steady state. However, if either the LED voltage, or bus voltage, or operating frequency is modified, the output current will also be modified. If the final goal is to obtain a constant LED current, the control circuit should be able to change the operating frequency to compensate variations in the bus voltage or in the LED characteristics.

Assuming that changes in LED or bus voltages are extremely slow compared to the converter dynamics, the steady-state equations can also be used to determine how the operating point is modified. Therefore, the linearization of the equations around the steady-state solution is made to analyze the LED current sensitivity against changes in $V_{\mathrm{BUS}}, V_{\mathrm{LED}}$, or ω.

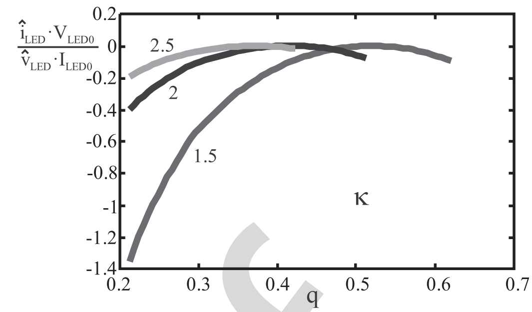

Fig. 12. LED current sensitivity against changes in LED voltage.

In Section IV, equations *F*1–*F*4 were obtained

$$R \cdot \omega \cdot C_P = F1\,(\alpha, q, \kappa) \tag{28}$$

$$R \cdot \omega \cdot C_A = F2\,(q, \kappa) \tag{29}$$

$$R \cdot \omega \cdot C_R = F3\,(\alpha, q, \kappa, \nu) \tag{30}$$

$$\frac{\omega \cdot L_R}{R} = F4\,(\alpha, q, \kappa, \nu)\,. \tag{31}$$

These four equations can be linearized to perform the small signal analysis. This way, the linearized matrix expression (32) is obtained, as shown bottom of the next page.

Symbol "∧" is used to denote a small signal variation of the affected variable and subindex "0" is used to indicate the steady-state value. To use a more compact notation, the 2×4 matrix on the left side is denoted as A, and the 4×4 matrix on the right side as B. This way, $\hat{\kappa}$ value can be expressed as

$$\begin{pmatrix} 0 & 0 & 1 & 0 \end{pmatrix} \cdot B^{-1} \cdot A \cdot \begin{bmatrix} \frac{\hat{R}}{R_0} \\ \frac{\hat{\omega}}{\omega_0} \end{bmatrix} = \hat{\kappa}. \tag{33}$$

As the final goal is to obtain the small signal variation of i_{LED} against changes in $V_{\mathrm{LED}}, V_{\mathrm{BUS}}$, and ω, the following variable changes are applied:

$$\hat{\kappa} = \kappa_0 \frac{\hat{v}_{\mathrm{BUS}}}{V_{\mathrm{BUS0}}} - \kappa_0 \frac{\hat{v}_{\mathrm{LED}}}{V_{\mathrm{LED0}}} \tag{34}$$

$$\frac{\hat{R}}{R_0} = \frac{\hat{v}_{\mathrm{LED}}}{V_{\mathrm{LED0}}} - \frac{\hat{i}_{\mathrm{LED}}}{I_{\mathrm{LED0}}}. \tag{35}$$

The combination of (33)–(35) provides all the curves depicted in Figs. 12–14. As shown in Fig. 12, there are certain combinations of *q* and κ where the LED current is not affected by small changes in the LED voltage. However, according to Fig. 13, changes in bus voltage always have a significant effect on the output current. Hence, if a current source behavior is desired, changes in bus voltage must be compensated. In the present work, this regulation is done by modifying the operating frequency. Assuming a linear behavior, the required gain between bus voltage and operating frequency to keep a constant LED current can be obtained using the charts from Figs. 13 and 14.

One of the most interesting characteristics of this control strategy is that if the nominal operating point is selected to meet

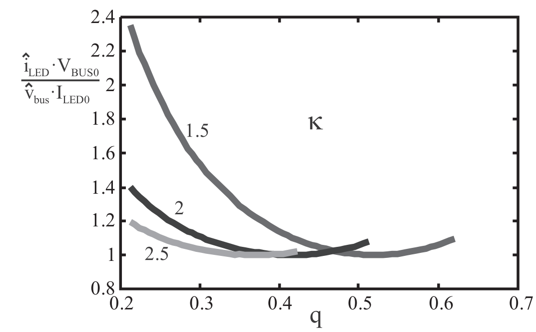

Fig. 13. LED current sensitivity against changes in bus voltage.

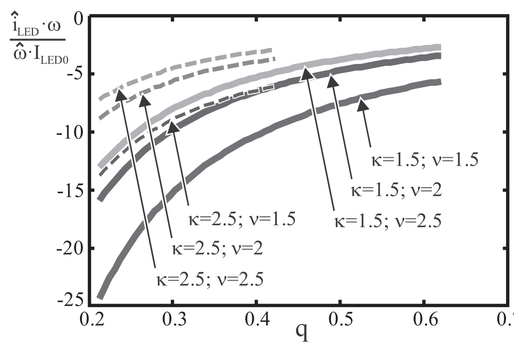

Fig. 14. LED current sensitivity against changes in switching frequency.

the following condition:

$$\frac{\hat{i}_{\mathrm{LED}} \cdot V_{\mathrm{LED0}}}{\hat{v}_{\mathrm{LED}} \cdot I_{\mathrm{LED0}}} = 0 \tag{36}$$

from Fig. 12, the converter will behave as a current source against small variations in LED voltage. Therefore, if two identical converters are supplied from the same input bus and driven using the same control signals, the current flowing through each LED will have a very small dependence on the output voltage, providing natural current equalization.

VI. Design Example and Experimental Results

In the proposed topology, there are five components that must be calculated to complete the design: capacitors C_P and C_A, resonant tank L_R–C_R, and input filter inductor L_F. This last element must be designed in order to minimize LED high-frequency ripple. All other components can be calculated using the charts shown in Figs. 9–11 as functions of six design parameters: $\delta, q, \kappa, \nu, \omega$, and R. Two of these parameters, in particular κ and R, can be obtained from the input bus voltage and the lamp characteristics. Parameter δ, as explained in Section III, is set to a tradeoff value of 10%.

TABLE I
Prototype Specifications

Basic circuit specifications			
Nominal input voltage	Input voltage excursion		Nominal frequency
160V	±30V (peak)		200 kHz
Output current	Nominal output voltage	Nominal output power	
0.5A	80V	40W	
LED lamp characteristics			
Model	Manufacturer	Nominal current	Number of LEDs
Oslon SSL80	Osram	0.8A	24
Selected design parameters			
α	q	κ	ν
30º	0.5	2	1.5
Circuit parameters			
C_P	C_A	C_R	MOS
1.3n	2.1nF	2.3nF	04N60S5
L_R	L_F		Diodes
408μH E30 3C96	2mH E30 3C96		MUR130
Control parameters			
t_{OFF}	t_{ON}		
$2.2\cdot10^{-6}$ s	$2.8\cdot10^{-6} - 5.9\cdot10^{-9}\cdot(V_{BUS} - 160)$ s		

To further illustrate the proposed design methodology, a laboratory prototype has been built and tested. The basic design parameters are summarized in Table I. The lamp consisted of 24 LEDs in series providing a nominal voltage of 80 V at 500 mA. The nominal input voltage was 160 V, giving a nominal κ of 2. According to Fig. 12, to eliminate the LED voltage effect on the output current for the selected κ, a q value of 0.42 should be chosen. However, between 0.31 and 0.52, changes in the output current will be ten times or less compared to LED voltage changes. In this design a q value of 0.5 has been used.

The resonant tank must be designed to operate above its natural resonant frequency, providing a pure inductive behavior at the switching frequency. The equivalent impedance of the resonant tank at the fundamental frequency can be obtained using Fig. 11. Parameter ν sets the ratio between L_R and C_R impedances. Higher values of ν lead to smaller inductance and higher capacitance in the resonant tank, but also to lower

$$\begin{bmatrix} F1(\alpha_0, q_0) & F1(\alpha_0, q_0) \\ F2(q_0, \kappa_0) & F2(q_0, \kappa_0) \\ F3(\alpha_0, q_0, \kappa_0, \nu_0) & F3(\alpha_0, q_0, \kappa_0, \nu_0) \\ -F4(\alpha_0, q_0, \kappa_0, \nu_0) & F4(\alpha_0, q_0, \kappa_0, \nu_0) \end{bmatrix} \cdot \begin{bmatrix} \frac{\hat{R}}{R_0} \\ \frac{\hat{\omega}}{\omega_0} \end{bmatrix} =$$

$$\begin{bmatrix} \frac{\delta F1(\alpha_0,q_0)}{\delta\alpha} & \frac{\delta F1(\alpha_0,q_0)}{\delta q} & 0 & 0 \\ 0 & \frac{\delta F2(q_0,\kappa_0)}{\delta q} & \frac{\delta F2(q_0,\kappa_0)}{\delta\kappa} & 0 \\ \frac{\delta F3(\alpha_0,q_0,\kappa_0,\nu_0)}{\delta\alpha} & \frac{\delta F3(\alpha_0,q_0,\kappa_0,\nu_0)}{\delta q} & \frac{\delta F3(\alpha_0,q_0,\kappa_0,\nu_0)}{\delta\kappa} & \frac{\delta F3(\alpha_0,q_0,\kappa_0,\nu_0)}{\delta\nu} \\ \frac{\delta F4(\alpha_0,q_0,\kappa_0,\nu_0)}{\delta\alpha} & \frac{\delta F4(\alpha_0,q_0,\kappa_0,\nu_0)}{\delta q} & \frac{\delta F4(\alpha_0,q_0,\kappa_0,\nu_0)}{\delta\kappa} & \frac{\delta F4(\alpha_0,q_0,\kappa_0,\nu_0)}{\delta\nu} \end{bmatrix} \cdot \begin{bmatrix} \hat{\alpha} \\ \hat{q} \\ \hat{\kappa} \\ \hat{\nu} \end{bmatrix}. \tag{32}$$

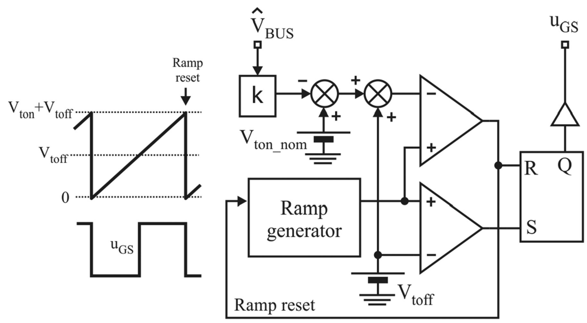

Fig. 15. Equivalent block diagram of the proposed control circuit.

TABLE II
EXPERIMENTAL RESULTS

With constant bus voltage			
V_{BUS} = 160V			
	Calculated	Simulated	Measured
I_{res} (rms)	0.7A	0.7A	0.69A
I_{LED}	0.5A	0.51A	0.49
V_{MOS} (max)	320V	357V	393V
Bus voltage with 30V ripple at 100Hz			
V_{BUS} = 130V			
	Estimated	Simulated	Measured
I_{res} (rms)	0.59A	0.52A	0.55A
I_{LED}	0.5A	0.49A	0.48
V_{MOS} (max)	207V	224V	253V
V_{BUS} = 190V			
	Estimated	Simulated	Measured
I_{res} (rms)	0.88A	0.82A	0.8
I_{LED}	0.5A	0.51	0.49
V_{MOS} (max)	420V	468V	490V

sensitivity against changes in the operating frequency (see Fig. 14). This characteristic increases the frequency excursion required for a given bus voltage ac ripple but it also reduces the sensitivity against changes in L_R and C_R. In this example, parameter ν was set to a tradeoff value of 1.5.

Using the linearization procedure described in Section V, the required frequency excursion to compensate an input voltage ripple of ±30 V at 100 Hz has been calculated. The maximum and minimum durations of the switch ON time required to maintain ZVS has been estimated using the same linear approach and it has been found that, at both maximum and minimum input voltages, there was margin to set a fixed OFF-time and control the operating frequency modifying only the switch ON time; thus, the proposed control was to linearly modify the ON-time according to the input voltage. The equivalent block diagram of the proposed control is shown in Fig. 15. The practical implementation was made using a dsPIC30F4012 microcontroller with an extremely simple control program. The microcontroller sampled the bus voltage at 10 kHz and adjusted the ON-time of the switch linearly according to the formula shown at the bottom of Table I. This formula provides a nominal switching frequency of 200 kHz.

The power topology and the proposed control have been also simulated using Psim 9.0 software. Table II shows a comparison between some of the results obtained using the fundamental approach, Psim simulation, and experimental measures. As can be seen, the biggest difference is found in the peak MOSFET voltage, where the harmonic content of the resonant current and parasitics in the circuit components have a higher effect.

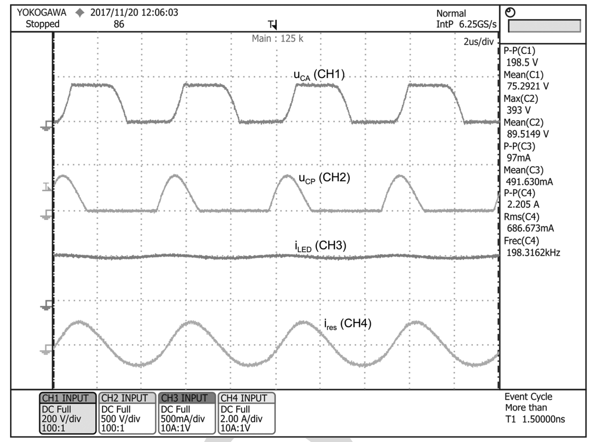

Fig. 16. Basic circuit waveforms at nominal bus voltage.

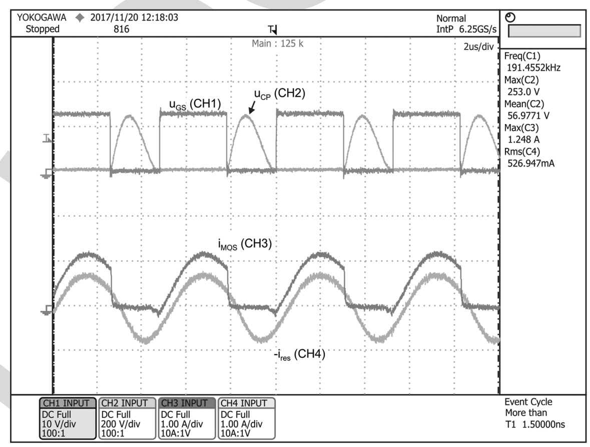

Fig. 17. Switching waveforms at 130 V bus voltage.

Fig. 16 shows the basic circuit waveforms of the laboratory prototype working with an input voltage of 160 V. Channels 1 and 2 show the $u_{\rm CA}$ and $u_{\rm CP}$ voltages, respectively. Channels 3 and 4 show the LED and the resonant currents. As can be seen, the experimental waveforms are quite similar to the expected signals. Fig. 17 shows the switching waveforms at a minimum bus voltage of 130 V. This is the worst-case condition for maintaining ZVS switching. It can be observed that the rising edge of the MOSFET gate signal ($u_{\rm GS}$) occurs when the MOSFET current ($i_{\rm MOS}$) is flowing through its intrinsic body diode.

After analyzing the behavior of the prototype at a constant input voltage, a 30 V sinusoidal ripple was added. The basic circuit waveforms obtained are shown in Fig. 18. The traces shown in the top half of the screen show the effect of the 100 Hz perturbation. Bottom half of the screen is used to show two magnified portions of the traces: left side with the maximum and right side with the minimum bus voltage. As can be seen, C_P capacitor is fully discharged in every cycle, as required for ZVS operation. The measured converter efficiency in this test has been 93%. Peak-to-peak LED current ripple at 100 Hz has

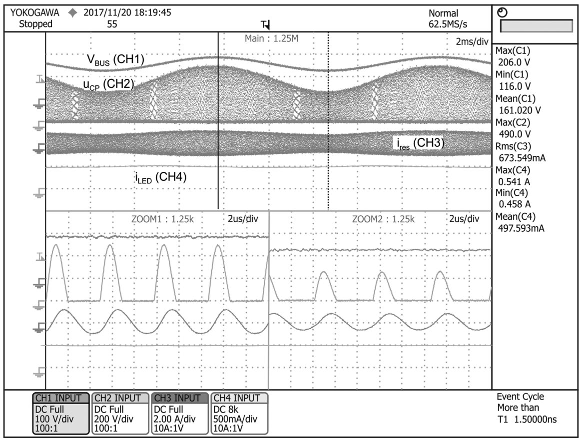

Fig. 18. Basic circuit waveforms with a 30 V peak voltage ripple at 100 Hz in the input bus.

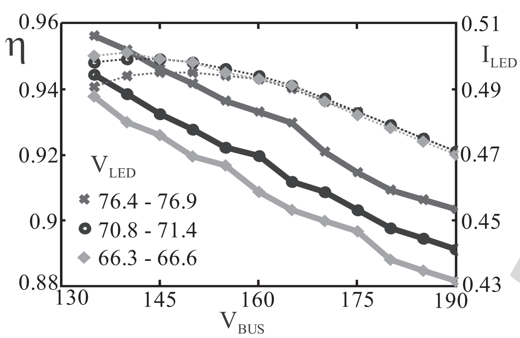

Fig. 19. Measured efficiency and LED current as a function of the input voltage and the LED voltage.

TABLE III
ESTIMATED LOSSES DISTRIBUTION

Nominal load (V_{LED} = 76.8V)			
V_{BUS} = 130V			
Mosfet	Lres	Diodes	Others
31%	27%	27%	15%
V_{BUS} = 160V			
Mosfet	Lres	Diodes	Others
22%	47%	19%	12%
V_{BUS} = 190V			
Mosfet	Lres	Diodes	Others
14%	70%	11%	5%

been 7.5%. This value complies with recommendations given in the IEEE PAR1789 Standard [25].

To verify the effect of LED voltage, the circuit was tested at a constant input voltage with three different loads. This was made by changing the number of diodes in the string. The basic results are summarized in Fig. 19. As can be seen, the converter efficiency depends on both the LED voltage and bus voltage, but LED voltage has a negligible effect on the output current.

In order to estimate how the losses were distributed in the converter, several Psim simulations were carried out considering the parasitics of all relevant components. As presented in Table III, the resonant inductance has the higher losses, especially at high bus input voltage.

VII. Conclusion

In this paper, a new power topology based on a class-E resonant inverter working as an LED current regulator was presented. This topology only required one controlled switch and was especially suited to operate at very high frequencies due to its extremely small switching losses.

The circuit behavior was analyzed using the fundamental approach. The analysis was oriented to obtain a set of charts that allowed a straightforward design and calculus of all circuit components. Based on the proposed procedure, a design example was presented and a laboratory prototype was built and tested. The circuit was optimized to reduce the effect of LED voltage in the output current. Bus voltage variations were compensated using a simple feedforward control that changed the ON-time of the switch linearly with the input voltage.

The prototype was tested with a peak-to-peak input ripple up to 37.5% at 100 Hz without losing ZVS commutations. The highest difference between calculated and experimental values was measured in the peak MOSFET voltage with a 17% deviation. This difference was due to the simplifications used in the analysis and intrinsic parasitics of the circuit components. All other measurements were in good agreement with calculated values.

References

[1] B. V. Lumileds Holding, "Evaluating the lifetime behavior of LED systems," *White Paper 20161201*, 2016. [Online]. Available: www.lumileds.com

[2] P. S. Almeida, D. Camponogara, M. Dalla-Costa, H. Braga, and J. M. Alonso, "Matching LED and driver life spans: A review of different techniques," *IEEE Ind. Electron. Mag.*, vol. 9, no. 2, pp. 36–47, Jun. 2015.

[3] B. Sun, X. Fan, C. Qian, and G. Zhang, "PoF-simulation-assisted reliability prediction for electrolytic capacitor in LED drivers," *IEEE Trans. Ind. Electron.*, vol. 63, no. 11, pp. 6726–6735, Jun. 2016.

[4] A. Shrivastava, M. H. Azarian, and M. Pecht, "Failure of polymer aluminum electrolytic capacitors under elevated temperature humidity environments," *IEEE Trans. Compon. Packag. Manuf. Technol.*, vol. 7, no. 5, pp. 745–750, May 2017.

[5] J. Garcia, A. J. Calleja, E. L. Corominas, D. Gacio, and J. Ribas, "Electronic driver without electrolytic capacitor for dimming high brightness LEDs," in *Proc. 35th Annu. Conf. IEEE Ind. Electron.*, Nov. 2009, pp. 3518–3523.

[6] G. Gindri Pereira, M. A. Dalla-Costa, J. M. Alonso, M. Flores De Melo, and C. Henrique Barriquello, "LED driver based on input current shaper without electrolytic capacitor," *IEEE Trans. Ind. Electron.*, vol. 64, no. 6, pp. 4520–4529, Jun. 2017.

[7] J. C. W. Lam and P. K. Jain, "Isolated ac/dc offline high power factor single-switch LED drivers without electrolytic capacitors," *IEEE J. Emerging Sel. Topics Power Electron.*, vol. 3, no. 3, pp. 679–690, Apr. 2015.

[8] M. Arias, D. G. Lamar, J. Sebastian, D. Balocco, and A. Aguissa Diallo, "High-efficiency LED driver without electrolytic capacitor for street lighting," *IEEE Trans. Ind. Appl.*, vol. 49, no. 1, pp. 127–137, Jan./Feb. 2013.

[9] B. White, H. Wang, Y. F. Liu, and X. Liu, "An average current modulation method for single-stage LED drivers with high power factor and zero low-frequency current ripple," *IEEE J. Emerging Sel. Topics Power Electron.*, vol. 3, no. 3, pp. 714–731, Sep. 2015.

[10] P. S. Almeida, J. M. Jorge, C. R. B. S. Rodrigues, G. M. Soares, D. P. Pinto, and H. A. C. Braga, "A novel method of current equalization in LED strings based on simple linear circuit," in *Proc. IEEE Symp. Ind. Electron.*, Jun. 2011, pp. 95–100.

[11] H. S. H. Chung and R. Zhang, "Paralleled LED strings: An overview of current-balancing techniques," *IEEE Ind. Electron. Mag.*, vol. 9, no. 2, pp. 17–23, Jun. 2015.

[12] J. K. Kim, J. B. Lee, and G. W. Moon, "Isolated switch-mode current regulator with integrated two boost LED drivers," *IEEE Trans. Ind. Electron.*, vol. 61, no. 9, pp. 4649–4653, Sep. 2014.

[13] J. Zhang, T. Jiang, and X. Wu, "A high-efficiency quasi-two-stage LED driver with multi-channel outputs," *IEEE Trans. Ind. Electron.*, vol. 64, no. 7, pp. 5875–5882, Jul. 2017.

[14] P. J. Liu and K. L. Peng, "Adaptive driving bus voltage and energy recycling control schemes for low-power ac-dc RGB-LED drivers," *IEEE Trans. Ind. Electron.*, vol. 64, no. 10, pp. 7741–7748, Oct. 2017.

[15] C. S. Moo, Y. J. Chen, and W. C. Yang, "An efficient driver for dimmable LED lighting," *IEEE Trans. Power Electron.*, vol. 27, no. 11, pp. 4613–4618, Nov. 2012.

[16] L. R. Nerone, "Analysis and design of a self-oscillating class E ballast for compact fluorescent lamps," *IEEE Trans. Ind. Electron.*, vol. 48, no. 1, pp. 151–160, Feb. 2001.

[17] F. del-Aguila-Lopez, P. Pala-Schonwalder, P. Molina, and A. Mediano-Heredia, "A discrete-time technique for the steady-state analysis of nonlinear class-E amplifiers," *IEEE Trans. Circuits Syst.*, vol. 54, no. 6, pp. 1358–1366, Jun. 2007.

[18] C. Bernal, E. Oyarbide, P. Molina, and A. Mediano, "Dynamic model of class-E inverter with multifrequency averaged analysis," *IEEE Trans. Ind. Electron.*, vol. 59, no. 10, pp. 3737–3744, Oct. 2012.

[19] Y. Wang, J. Huang, W. Wang, and D. Xu, "A single-stage single-switch LED driver based on class-E converter," *IEEE Trans. Ind. Appl.*, vol. 52, no. 3, pp. 2618–2626, May/Jun. 2016.

[20] T. Suetsugu and M. K. Kazimierczuk, "Diode peak voltage clamping of class E amplifier," in *Proc. 37th Conf. IEEE Ind. Electron. Soc.*, Nov. 2011, pp. 1318–1322.

[21] J. Ribas, J. A. Martin, J. Garcia, J. Cardesin, A. J. Calleja, and M. Rico-Secades, "Fluorescent lamp ballast based on a class-E resonant inverter using a piezoelectric transformer," in *Proc. Conf. Rec. IEEE Ind. Appl. Conf. 41st IAS Annu. Meeting*, vol. 1, Oct. 2006, pp. 252–256.

[22] J. Ribas, J. Garcia, J. Cardesin, M. Dalla-Costa, A. J. Calleja, and E. L. Corominas, "High frequency electronic ballast for metal halide lamps based on a PLL controlled class E resonant inverter," in *Proc. Conf. Rec. IEEE Power Electron. Spec. Conf.*, Jun. 2005, pp. 1118–1123.

[23] L. Li, Y. Gao, P. K. T. Mok, I. M. Sun, and N. Park, "A 16–28-W 92.8%-efficiency monolithic quasi-resonant LED driver with constant-duty-ratio frequency regulator," *IEEE Trans. Circuits Syst.*, vol. 62, no. 12, pp. 1199–1203, Dec. 2015.

[24] J. M. Alonso, A. J. Calleja, J. Ribas, E. Lopez-Corominas, and M. Rico-Secades, "Evaluation of a novel single-stage high-power-factor electronic ballast based on integrated buck half-bridge resonant inverter," in *Proc. IEEE Appl. Power Electron. Conf. Expo.*, Feb. 2000, pp. 610–616.

[25] *Recommended Practices for Modulating Current in High Brightness LEDs for Mitigating Health Risks to Viewers, IEEE Standard PAR1789*, Jun. 2015.

[26] Y. Wang, Y. Guan, K. Ren, W. Wang, and D. Xu, "A single-stage LED driver based on BCM boost circuit and LLC converter for street lighting system," *IEEE Trans. Ind. Electron.*, vol. 62, no. 9, pp. 5446–5457, Sep. 2015.

[27] Y. Wang, N. Qi, Y. Guan, C. Cecati, and D. Xu, "A single-stage LED driver based on SEPIC and LLC circuits," *IEEE Trans. Ind. Electron.*, vol. 64, no. 7, pp. 5766–5776, Jul. 2017.

[28] H. Dong, X. Xie, L. Jiang, Z. Jin, and X. Zhao, "An electrolytic capacitor-less high power factor LED driver based on a 'one-and-a-half stage' forward-flyback topology," *IEEE Trans. Power Electron.*, vol. 33, no. 2, pp. 1572–1584, Feb. 2018.

Javier Ribas (S'97–M'04–SM'12) was born in Milwaukee, WI, USA, in 1971. He received the M.Sc. and Ph.D. degrees in industrial engineering from the University of Oviedo, Gijon, Spain, in 1995 and 2001, respectively.

Since 1996, he has been with the Department of Electrical Energy, University of Oviedo, where he is currently an Associate Professor. He is an Active Member of the Efficient Energy Conversion, Industrial Electronics and Lighting Research Group, University of Oviedo. He is a coauthor of more than 20 journal papers and more than 70 international conference papers in industrial and power electronics. His research interests include electronic lighting systems, solid-state lighting, switched-mode power supplies, and high-power-factor rectifiers.

Pablo J. Quintana-Barcia (S'13–M'16) was born in Tapia de Casariego, Spain, in 1987. He received the M.Sc. degree in electrical engineering and the Ph.D. degree in power electronics from the University of Oviedo, Gijon, Spain, in 2011 and 2015, respectively.

In September 2011, he joined the Electrical and Electronic Engineering Department, University of Oviedo, where he is currently an Assistant Professor. His research interests include power electronics and control for industrial, grid support, and lighting applications.

Jesus Cardesin (S'01–A'03–M'04) was born in Oviedo, Spain, in 1970. He received the M.Sc. and Ph.D. degrees in electrical engineering from the University of Oviedo, Gijon, Spain, in 1995 and 2002, respectively.

In 1999, he joined the Electrical and Electronic Department, University of Oviedo, where he was an Assistant Professor from 1999 to 2007 and has been an Associate Professor since 2007. His current research interests include industrial electronics and power electronics, resonant converters, electronic ballasts, discharge lamps modeling, dc–dc converters, power factor correction, LED lighting, and renewable energy.

Antonio J. Calleja (S'96–A'98–M'04–SM'12) was born in Leon, Spain, in 1964. He received the B.S., M.Sc., and Ph.D. degrees from the University of Oviedo, Gijon, Spain, in 1987, 1995, and 2000, respectively. Q2

He is currently with the University of Oviedo, where he was an Assistant Professor from 1995 to 2001 and has been an Associate Professor since 2002. He is also with the Efficient Energy Conversion, Industrial Electronics and Lighting Research Group, working on the development of power electronic systems for renewable generation systems, electronic switching power supplies, lighting electronics, and digital control for power electronics. His research interests include power electronics for renewable generation systems; bidirectional converters; dc–dc converters and power factor correction stages; switching-mode power supplies; modeling of light sources, inverters, and igniters for high-intensity discharge lamps; and electronic drivers for high-brightness light-emitting diodes.

Emilio Lopez Corominas (M'97) was born in Oviedo, Spain, in 1965. He received the M.Sc. and Ph.D. degrees in electrical engineering from the University of Oviedo, Gijon, Spain, in 1992 and 1999, respectively.

From 1993 to 2001, he was an Assistant Professor with the Electrical and Electronic Department, University of Oviedo, where since 2001 he has been Associate Professor. His research interests include electronic systems for lighting and renewable energy systems, high-frequency electronic ballasts, lamp modeling, electronic drivers for high-brightness LEDs, high-frequency switching converters, power factor correction converters, industrial control systems, and digital control for power electronics.